Journal of proteome research

pubs.acs.org/jpr Article

Unraveling the Metabolic Alterations Induced by Zika Infection in Prostate Epithelial (PNT1a) and Adenocarcinoma (PC-3) Cell Lines

Jeany Delafiori, Alessandra V. de S. Faria, Arthur N. de Oliveira, Geovana M. Sales, Flávia Luísa Dias-Audibert, and Rodrigo R. Catharino*

Cite This: *J. Proteome Res.* 2023, 22, 193−203 Read Online

ACCESS | Metrics & More | Article Recommendations | Supporting Information

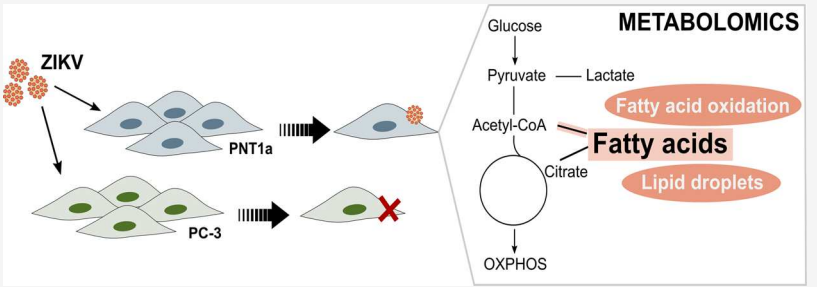

ABSTRACT: The outbreak of Zika virus infection in 2016 led to the identification of its presence in several types of biofluids, including semen. Later discoveries associated Zika infection with sexual transmission and persistent replication in cells of the male reproductive tract. Prostate epithelial and carcinoma cells are favorable to virus replication, with studies pointing to transcriptomics alterations of immune and inflammation genes upon persistence. However, metabolome alterations promoted by the Zika virus in prostate cells are unknown. Given its chronic effects and oncolytic potential, we aim to investigate the metabolic alterations induced by the Zika virus in prostate epithelial (PNT1a) and adenocarcinoma (PC-3) cells using an untargeted metabolomics approach and high-resolution mass spectrometry. PNT1a cells were viable up to 15 days post ZIKV infection, in contrast to its antiproliferative effect in the PC-3 cell lineage. Remarkable alterations in the PNT1a cell metabolism were observed upon infection, especially regarding glycerolipids, fatty acids, and acylcarnitines, which could be related to viral cellular resource exploitation, in addition to the over-time increase in oxidative stress metabolites associated with carcinogenesis. The upregulation of FA20:5 at 5 dpi in PC-3 cells corroborates the antiproliferative effect observed since this metabolite was previously reported to induce PC-3 cell death. Overall, Zika virus promotes extensive lipid alterations on both PNT1a and PC-3 cells, promoting different outcomes based on the cellular metabolic state.

KEYWORDS: *mass spectrometry, Zika virus, prostate cells, prostate cancer, metabolomics*

INTRODUCTION

Zika virus (ZIKV) is a flavivirus from the Flaviviridae family first detected in 1947 in Uganda.[1] A self-limiting febrile disease was reported for this arbovirus in 2015 during the outbreak in the Americas and Pacific Islands. At that time, Zika virus infection was associated with several cases of Guillain−Barré syndrome and congenital microcephaly.[2,3] Consequently, Zika infection-related outcomes came in the spotlight for the first time.

The gained visibility of the Zika epidemiology importance[3] was supported by reports of Zika virus's impact on neuronal growth impairment and its oncolytic potential in neural tumor management.[4−8] Zika neurotropism and replication were characterized by an interruption in the cell cycle and cell death induction.[6−10] In addition to nervous system tropism, ZIKV can be transmitted sexually; viral RNA was detected in semen for more than 60 days after symptom onset, being accompanied by prostatitis in some cases.[11−13] In this context, the assessment of male reproductive systems' cells to ZIKV infection susceptibility was amplified; findings of the potential involvement of human prostate cells as Zika replication sites have shown stable viral RNA concentrations up to 14 days post infection.[12] Short-term ZIKV infection in prostate cancer cells DU-145 also demonstrated high and consistent virus titter during 72 h.[7] Izuagbe et al. observed that ZIKV-persistent infection in prostate epithelial cells led to transcriptomics alterations in genes involved in antiviral and immune responses, such as viral recognition, expression of cytokines,

Received: October 4, 2022
Published: December 5, 2022

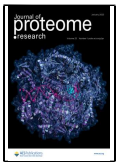

and interferons.[14] Additionally, Machado et al. presented that miRNAs generated during human prostate cell infection with a Brazilian ZIKV strain had genes that were involved in inflammation, immunity, cell survival, and proliferation as in silico-predicted targets.[15]

Overall, the cell machinery is remodeled during flavivirus replication, especially for the use of cell substrates for replication and lipid biogenesis.[16] In metabolic terms, prostate cells are known to have a peculiar inefficient energy metabolism in the basal state. Prostate cells rewire citrate production to excretion by inhibiting citrate conversion to isocitrate in the tricarboxylic acid (TCA) cycle.[17−19] This results in the accumulation of citrate and, as a consequence, less production of energy through oxidative phosphorylation (OXPHOS) and lipid synthesis.[18,19] However, during the malignant process, mitochondrial aconitase is less inhibited, leading to the use of accumulated citrate for energy production via OXPHOS, altered fatty acid (FA) metabolism, and lipid droplet (LD) accumulation.[17−21] As the tumor progresses, metastatic cells further decrease the use of OXPHOS, being characterized by glucose consumption and lactate production, known as the Warburg effect.[17,19] Considering the characteristics of prostate normal cell and cancer cell metabolism and the flavivirus replication, the impact of Zika persistent infection in human epithelial prostate cell and cancer cell metabolism and proliferation needs further investigation.

Studies to assess Zika infection mechanisms are important to advance the understanding of transmission prevention and clinical manifestations,[6,8,9,22,23] to address challenges facing new approaches for diagnosis, treatment, and vaccines,[24−26] and the virus use in Zika-related therapies.[4,5,10] This comprehension can be further extended by metabolomics using high-resolution mass spectrometry,[10,16,26−28] which aims to assess, at the low-weight-molecular level, the metabolic alterations that result in cell phenotype. Therefore, by associating the multifactorial characteristics of Zika infection to the susceptibility of prostate cells to persistent infection, this study aims to employ an untargeted metabolomic approach for the investigation of metabolic alterations induced by Zika virus in epithelial prostate cells (PNT1a) and prostate adenocarcinoma (PC-3) at short- and long-term exposure.

EXPERIMENTAL SECTION

Zika Strain and Cell Culture

The Brazilian ZIKV strain (BeH823339, GenBank KU729217) was isolated from a patient in 2015 at the Evandro Chagas Institute (Pará state, Brazil) and kindly provided by Prof. Dr Edison Durigon (University of São Paulo, USP). The ZIKV strain stock was maintained at −80 °C in the Laboratory of Emerging Viruses (Institute of Biology, UNICAMP). Before cellular assays, viral stock titer was determined by a plaque assay in Vero cells (PFU/mL).

Human prostatic immortalized cell line (PNT1a) and human prostate adenocarcinoma cell line (PC-3) were kindly provided by the In vitro Bioassays and Signal Transduction lab (Institute of Biology, UNICAMP). Cells were routinely grown at 4 × 10^4 cells/cm^2 density in a RPMI-1640 medium supplemented with 100 U/mL penicillin, 100 μg/mL streptomycin, and fetal bovine serum (FBS) 10% (Gibco, Thermo Fisher Scientific) and propagated at 37 °C in an 85% humidified and 5% CO_2 atmosphere. All lines were routinely checked for mycoplasma.

Colony Formation Assay

PNT1a and PC-3 colony formation assays were performed by seeding 2.8 × 10^3 cells/well in a six-well plate. Cells were maintained at 37 °C in an 85% humidified and 5% CO_2 atmosphere for 24 h to adhere. Cells were exposed to ZIKV multiplicity of infection (MOI) of 1 and 5, and together with mock cells, they were cultured for 15 days in an incubator (37 °C in an 85% humidified and 5% CO_2 atmosphere). The culture medium was topped up on days 3, 7, and 10. After 15 days, the supernatant was removed and cells were washed with PBS and fixed and stained for 30 min with crystal violet 5% (methanol/water). The solution was removed, and the cells were washed three times with water. Representative images were acquired with a phase-contrast microscope (Nikon, Japan), and colonies were counted using ImageJ (NIH).

Viability Assay

The cell viability assay was conducted by measuring the cell capacity in reducing MTT (3-(4,5-dimethylthiazol-2-yl)-2,5-diphenyltetrazolium bromide). PC-3 and PNT1a cells were seeded in a 96-well plate at 2.8 × 10^3 cell/well density in triplicate. After 24 h at 37 °C and 5% CO_2, cells were exposed to ZIKV MOI 1, and together with mock cells, they were maintained in a culture for 1, 2, and 3 days. The cell supernatant was removed and replaced by 100 μL/well of an MTT solution (0.5 mg/mL, in an FBS-free culture medium, sterile-filtered). After incubation for 3 h at 37 °C in an 85% humidified and 5% CO_2 atmosphere, the medium was removed, and 100 μL/well ethanol was added to solubilize the formazan. The microplates were shaken at a speed of 100 rpm for 10 min (Labnet orbit 1000) to solubilize the formazan produced. Absorbance was measured at λ = 570 nm in a microplate reader spectrophotometer (Synergy HT, BioTek). Cell viability was calculated using mock cell absorbance as reference, and graphs were generated using GraphPad Prism 5.0.

Metabolomics Assay

PNT1a and PC-3 cells were seeded at 4.2 × 10^3 cells/well density in 24-well plates and kept at 37 °C in an 85% humidified and 5% CO_2 atmosphere. After 24 h, cells were exposed to the ZIKV strain at MOI 1. Mock cells were kept at the same conditions and time points, except for the exposure to ZIKV. The cell culture medium was topped up on days 3, 7, and 10 according to each time point. PNT1a cells were harvested at time points of 5, 10, and 15 days post infection (dpi), while PC-3 cells were collected at 5 dpi. The culture medium was carefully removed, and cells were washed with a solution of NaCl (0.9%) and scraped from wells to a plastic tube. Cell suspensions were centrifuged for 5 min, 300*g*, at 4 °C to allow pellet formation. The supernatant was discarded, and the cell pellet was resuspended in 200 μL of ice-cold tetrahydrofuran and homogenized for 30 s. Additionally, 800 μL of ice-cold methanol was added. The cell suspension was homogenized, sonicated for 5 min, and centrifuged for 5 min, 1230*g*, at 4 °C. A 10 μL aliquot of the supernatant was diluted in 980 μL of methanol ionized with 1 μL of formic acid. Each sample was diluted into two preparation duplicates for analysis.

Mass Spectrometry Analysis and Metabolite Annotation

The extracted samples were directly infused in a HESI-Q Exactive Orbitrap (Thermo Scientific, Germany), with a resolution of 140,000 FWHM. Mass spectral data were acquired for each sample with five technical replicates using

https://doi.org/10.1021/acs.jproteome.2c00630
J. Proteome Res. 2023, 22, 193−203

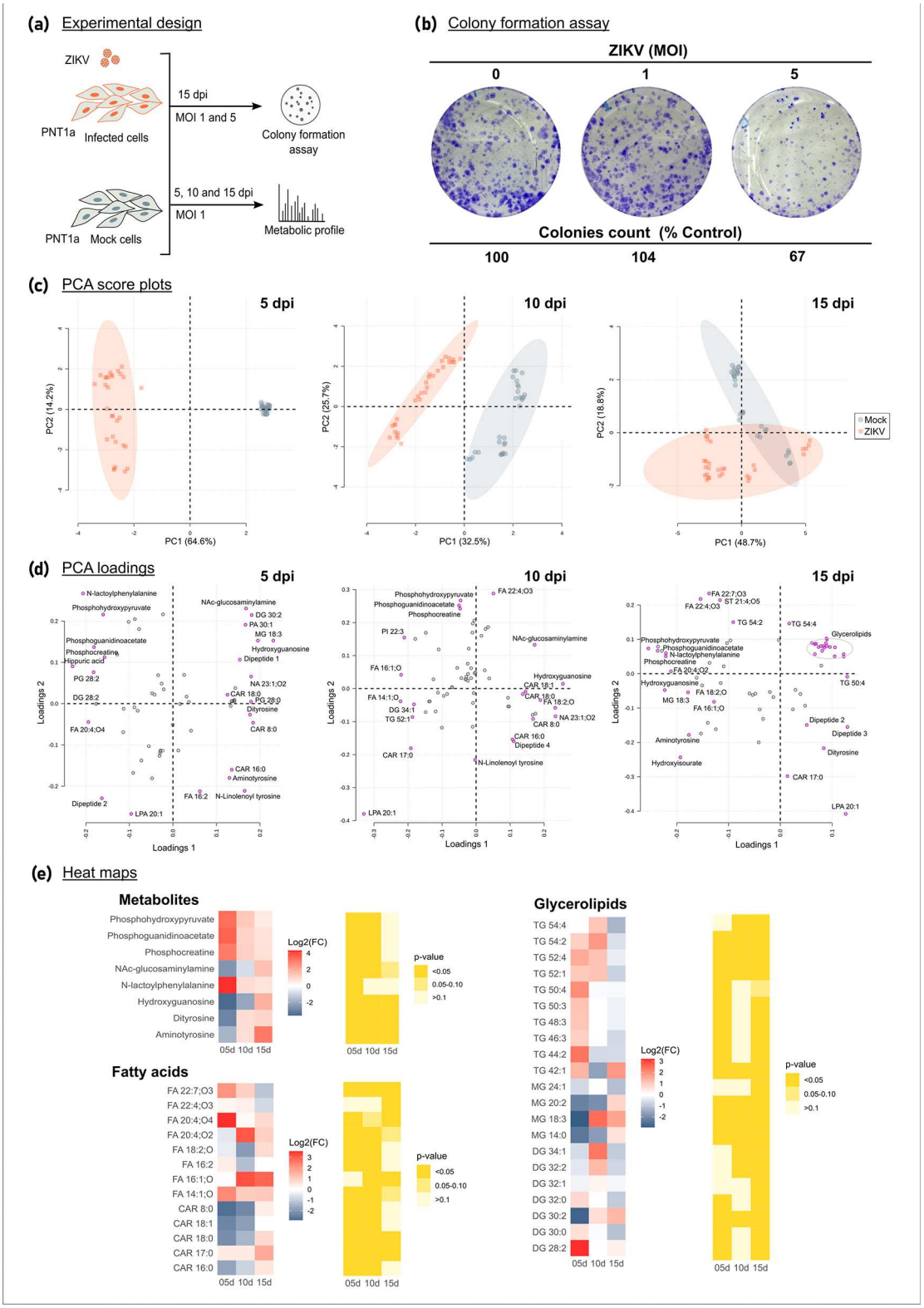

Figure 1. Metabolomics study to investigate PNT1a cell proliferation and metabolism during ZIKV-persistent infection. (A) Experimental design comprising a colony formation assay and cell harvesting for metabolomics analysis. (B) Colony formation assay of PNT1a upon Zika infection with MOI 1 and 5 compared to mock cells, maintained in a culture for 15 days. (C) PCA score plots at 5, 10, and 15 dpi time points showing the differentiation between PNT1a-infected cells and mock cells. (D) PCA loadings highlighting metabolites that mostly contributed to the conditions differentiated in PCA score plots. (E) Heat maps displaying the intensity levels ($\log_2$ FC) and significance (p-value < 0.05) of selected metabolites at 5, 10, and 15 dpi of PNT1a cells. The FC ratio compares infected cells over mock cells; positive $\log_2$(FC) (in red) corresponds to metabolites increased in ZIKV-infected cells, while negative $\log_2$(FC) (in blue) corresponds to decreased metabolites. Abbreviations: CAR, acylcarnitine; DG, diacylglycerol; FA, fatty acid; MG, monoacylglycerol; TG, triacylglycerol. Metabolites are subjected to isomers.

https://doi.org/10.1021/acs.jproteome.2c00630
J. Proteome Res. 2023, 22, 193−203

the positive ion mode and mass range from 175 to 1000m/z. The instrument was tuned with the following parameters: HESI 33 °C, flow rate 10 μL/min, capillary temperature 320 °C, spray voltage 3.7 kV, sheath gas flow of 5 (arbitrary units), RF-lens 50, AGC-target 1 × 106, and 50 scans/acquisition. XCalibur 3.0.63 software (Thermo Scientific, Germany) was used to visualize spectral data. Mass-to-charge (m/z) values were annotated using exact mass with accuracy <5 ppm when compared to the METLIN database (Scripps Center for Metabolomics, La Jolla, CA − www.metlin.scripps.edu). Additional databases such as LIPIDMAPS (University of California, San Diego, CA—www.lipidmaps.org), HMDB (Human Metabolome database - www.hmdb.ca), and Kegg (Kyoto Encyclopedia of Genes and Genomes - www.genome.jp/kegg) as well as literature search assisted with marker annotation and biological function assessment.

Data Analysis

Mass spectra data of cells infected with Zika virus at three different exposure times (5, 10, and 15 dpi) were compared to their respective mock cells. Mass signals were aligned, filtered (interquartile), normalized by a pooled sample from the control group (PQN), and transformed (logarithm base 10) prior to multivariate statistical analysis using partial least-squares discriminant analysis (PLS-DA) on the MetaboAnalyst 5.0 web server (www.metaboanalyst.ca).[29] For each comparison of ZIKV and mock cells at each time point, a VIP score list > 1.1 was used to select discriminant m/z values for annotation (described in the section above). Annotated data sets were used to project a principal component analysis (PCA) score plot and loadings to observe group differentiation and marker contribution. The significance of markers' intensity variation was assessed by a differential analysis, where fold changes (FCs) of logarithmic transformed data (ZIKV/Mock cells) at each time point were compared, and a p-value (FDR-adjusted) was attributed. Volcano plots of markers with FC > 1.5 and a p-value < 0.05 illustrate markers considered significant for the conditions. Log_2(FC) values provided for each metabolite and their respective significance allowed the comparison of time points through a heat map analysis. Plots were generated with R coding.

RESULTS

Metabolomics of ZIKV Infection Persistence in PNT1a Cells

Zika virus is known to infect several types of human cells, including epithelial, stromal, and prostate organoids.[12,30] Here, we aim to demonstrate that the normal human epithelial prostate cell (PNT1a) remains viable upon ZIKV infection, leading to metabolic changes during Zika infection persistence, which is not well characterized. Therefore, we performed colony formation assays and untargeted metabolomics analysis using high-resolution mass spectrometry, as illustrated in Figure 1A. A colony formation assay was used to evaluate the influence of ZIKV multiplicity of infection (MOI) of 1 and 5 in PNT1a cells' proliferation when compared to noninfected cells (Mock). Considering a persistent infection of 15 days, we observed that cell exposure to ZIKV MOI 1 did not substantially affect proliferation. As a result, a colony count of 104% compared to the control indicates the maintenance of cell viability and function upon persistent infection for 15 days (Figure 1B). However, upon MOI increase to 5, a decrease to 67% in colony count was observed.

Considering the maintenance of cell viability upon infection with ZIKV MOI 1, we performed a metabolomics assay where harvested PNT1a mock and ZIKV-infected cells were extracted with polar organic solvents, ionized, and directly infused in a high-resolution mass spectrometer. Ion signals ranging from 175 to 1000m/z were processed as described in the Methods section. Data were analyzed using multivariate statistical analysis through PLS-DA to discriminate between mock and ZIKV-infected groups (Supplementary Figure S1). For each time point, 5, 10, and 15 days post infection (dpi), a list of ions ranked by importance was used as the basis for metabolite annotation. A total of 62 metabolites were annotated by combining the three time points (Table S1). Fatty acids, carnitines, and glycerolipids were among the annotated lipid classes, in addition to small metabolites such as phosphohydroxypyruvate, phosphocreatine, N-lactoylphenylalanine, hydroxyguanosine, and dityrosine.

Together, these annotated markers supported and validated the differentiation of mock from ZIKV-infected PNT1a cells at 5, 10, and 15 dpi using unsupervised principal component analysis (Figure 1C). At each time point, the PCA score plot provided a high explanation of variability through components, with 78.8% (PC1 + PC2) for 5 dpi, 58.2% for 10 dpi, and 67.5% for 15 dpi. PCA loadings (Figure 1D) show the metabolites with the greatest effect on each component (loadings close to −1 or 1). In the first few days of infection (5 dpi), ZIKV-infected cells were characterized mainly by the variation of phosphohydroxypyruvate, phosphocreatine, N-lactoylphenylalanine, phosphoguanidinoacetate, and lysophosphatidic acid (LPA 20:1) ions' intensity. In addition to these markers, hydroxylated fatty acids (FA 16:1;O, and FA 14:1;O) influenced the differentiation between PNT1a ZIKV-infected cells and mock cells at 10 dpi. Notably, at 15 dpi, we observed a pronounced variation in the intensities of the glycerolipid class.

Aiming to qualitatively assess how much each marker contributed to these results, fold changes >1.5 for ZIKV-infected PNT1a cells and PNT1a mock cells at each time point were compared, and a p-value (FDR-adjusted) was attributed, as shown in the volcano plots (Supplementary Figure S2 and Table S1). Log_2 FC > 1 indicates a metabolite increase in PNT1a ZIKV-infected cells, while log_2 FC < 1 indicates a decrease. Heat maps using these results are displayed in Figure 1E. At 5 dpi, phosphohydroxypyruvate (log_2 FC 3.33, p-value < 0.05), phosphocreatine (log_2 FC 3.07, p-value < 0.05), phosphoguanidinoacetate (log_2 FC 3.54, p-value < 0.05), and N-lactoylphenylalanine (log_2 FC 4.32, p-value < 0.05) intensities were found elevated in infected cells compared to the control. However, the replication persistence promotes a shift in these metabolites' distribution across time points, going to normality, while a change from decreased to increased intensities of hydroxyguanosine, dityrosine, and aminotyrosine in infected cells is observed. Remarkably, few species of triacylglycerols (TG) and diacylglycerol (DG) were upregulated at 5 dpi, in contrast to the decreased intensities of monoacylglycerols (MG). However, with time, results show a general downregulation of TG species, while MG species increase.

Differences between PNT1a and PC-3 Metabolism upon ZIKV Infection

The workflow for the comparison of PNT1a and prostate adenocarcinoma cells' (PC-3) response to Zika infection was

https://doi.org/10.1021/acs.jproteome.2c00630
J. Proteome Res. 2023, 22, 193−203

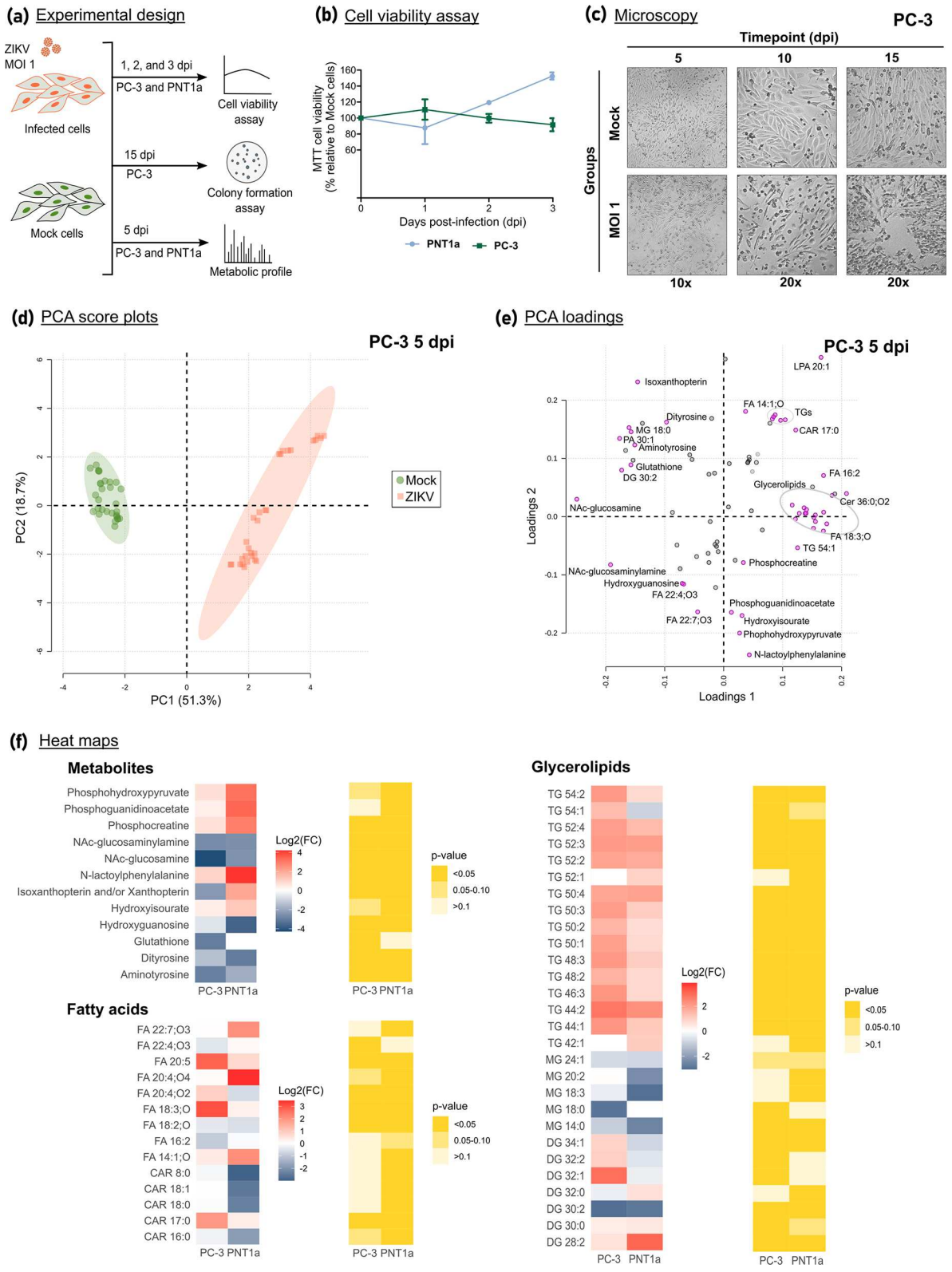

Figure 2. Metabolomics study to compare PNT1a and PC-3 cell proliferation and metabolism upon short-term Zika infection. (A) Experimental design comprising the cell viability assay (MTT), colony formation assay, and metabolomics analysis. (B) Cell viability assay using MTT at 1, 2, and 3 dpi showing a trend of PC-3 proliferation inhibition. (C) Brightfield microscopy images acquired during colony formation assay at 5, 10, and 15 dpi, showing PC-3 cell morphology loss and an increase in the number of dead cells. (D). PCA score plot of PC-3 at 5 dpi showing the differentiation between infected cells and mock cells. (E) PCA loadings highlighting metabolites that mostly contributed to the conditions differentiated in the PCA score plot. (E) Heat maps displaying the intensity levels ($\log_2$ FC) and significance (p-value < 0.05) of selected metabolites at 5 dpi for both PNT1a and PC-3 cells. FC ratio comparing infected cells with mock cells; positive $\log_2$(FC) (in red) corresponds to metabolites increased in ZIKV-infected cells, while negative $\log_2$(FC) (in blue) corresponds to decreased metabolites. Abbreviations: CAR, acylcarnitine; DG, diacylglycerol; FA, fatty acid; MG, monoacylglycerol; TG, triacylglycerol. Metabolites are subjected to isomers.

https://doi.org/10.1021/acs.jproteome.2c00630
J. Proteome Res. 2023, 22, 193−203

composed of a cell viability assay using MTT, a colony formation assay, and metabolomics analysis (Figure 2A). The cell viability assay at time points 1, 2, and 3 dpi shows the trend of decreasing PC-3 cell viability, in contrast to the maintenance of PNT1a cell proliferation (Figure 2B). Considering the colony formation assay with ZIKV MOI 1, PC-3 cell proliferation was completely inhibited within 15 days, and cells loosely detached from dish plates upon crystal violet treatment. This observation indicated that in addition to the susceptibility to ZIKV infection, PC-3 cell viability was compromised upon persistent replication. A deeper look with brightfield microscopy at 5, 10, and 15 dpi (Figure 2C) shows a progressive loss of the PC-3 cells' characteristic elongated morphology with an increase in dead cells.

Considering the vulnerability of PC-3 cells to ZIKV infection when compared to PNT1a, the time point of 5 dpi was considered for metabolomics evaluation. As previously stated, cell extracts were directly infused into a high-resolution mass spectrometer. Data were processed and analyzed using PLS-DA (Supplementary Figure S3) to differentiate between PC-3 ZIKV-infected cells and mock cells at the 5 dpi time point and rank the most important variables (m/z) for annotation. A combined table describing annotated markers for PC-3 and PNT1a at 5 dpi is provided in the Supplementary material Table S2. These markers are important to differentiate mock cells from ZIKV-infected cells through unsupervised analysis (PCA) (Figure 2D) with an explained variance of 70% (PC1 + PC2). PCA loadings show the important contribution of fatty acids (FA16:2 and FA18:3;O), N-acetyl-glucosaminyl-amine, N-acetyl-glucosamine, and the glycerolipid class in general, especially triacylglycerols (Figure 2E).

A volcano plot using $\log_2$(FC) > 1.5 and p-value <0.05 (FDR-adjusted) is shown in Supplementary Figure S4. Selected metabolites were included in heat maps for qualitative evaluation of the two cell lines' response to short-term Zika infection (Figure 2F). N-Lactoylphenylalanine, phosphocreatine, and isoxanthopterin/xanthopterin were found to be less increased in PC-3 when compared to PNT1a. N-Acetylglucosamine was found to be downregulated in both cell types, being more intensively decreased in PC-3 cells. Additionally, FA 20:5 and FA 18:3;0 were differential metabolites when compared to PNT1a, while several other TG species were enhanced at 5 dpi, potentially reflecting the lipid accumulation characteristic of prostate cancer cells.

DISCUSSION

Evidence of the sexual transmission and long-term viral load in the semen of Zika virus generated a series of studies to address the impact of ZIKV replication on the male reproductive system.[11−13] Prostate cells were confirmed to favor ZIKV infection and indicated it as a potential replication reservoir;[7,12] however, only a few studies focused on addressing the mechanism of persistence in prostate cells.[14,15] In this study, our contributions toward understanding ZIKV persistence in prostate cells include (i) a demonstration of how ZIKV infection impacts cell viability of a prostate epithelial cell line (PNT1a) and a prostate adenocarcinoma cell line (PC-3) in the short and long term; (ii) the metabolic alterations induced by ZIKV-persistent replication in PNT1a during a 15 day assay; and (iii) the metabolic differences between the short-term infection in PNT1a and PC-3. Therefore, this is the first metabolomic study based on high-resolution mass spectrometry designed to investigate Zika replication persistence in prostate cells.

ZIKV Effects on Prostate Cells Is Cell-Type Dependent

Recently, Machado et al. demonstrated that PNT1a cells are permissive to the Brazilian ZIKV strain.[15] Prostate mesenchymal cells and epithelial adenocarcinoma cells were previously reported to be susceptible to Zika persistent replication, with the detection of stable concentrations of viral RNA in a 14 day assay.[12] ZIKV RNA detection in prostate cells was further extended to 30 dpi in vitro. Izuagbe reported no difference in epithelial cell viability up to 30 days at low MOI infection, regardless of the strain.[14] Similarly, we demonstrated that prolonged *in vitro* ZIKV infection of PNT1a at low multiplicity (MOI) did not affect cellular proliferation in 15 days. Even though the PNT1a ZIKV-infected cell viability was comparable to that of mock cells, substantial alterations in cell metabolism were observed.

Fatty acids and oxidized fatty acids (oxylipins) were found to be remarkably altered upon prostate epithelial cell ZIKV infection (Figure 1E). Oxylipins can be generated enzymatically and nonenzymatically mediated by ROS, showing increased and decreased levels according to molecule specie and time point. These bioactive lipids carry out important roles as anti-inflammatory and proinflammatory agents. For example, we observed a significant decrease in FA 18:2;O at 5 and 10 dpi in infected cells compared to the control with a slight increase at 15 dpi. This molecule can correspond to 9- and/or 13-HODE (hydroxy-decadienoic acid), which exerts proinflammatory and anti-inflammatory properties, respectively. Both oxylipins were found to increase in the placenta infected with ZIKV and in plasma of newborns with ZIKV-induced microcephaly.[31,32] In a study with blood donors, Catala et al. demonstrated that FA and oxylipin concentrations in red blood cells infected by ZIKV are time-dependent, with HODE intensities increasing after 10 dpi.[33]

Moreover, we detected markers associated with enhanced oxidative stress. Dityrosine, aminotyrosine, and hydroxyguanosine intensities in ZIKV-infected cells increase in prolonged cellular infection (15 dpi). The nitration of tyrosine is a protein posttranslational modification promoted by the presence of ROS (reactive oxygen species), leading to functional alterations; their increase is associated with inflammation-related diseases.[34,35] ROS also interacts with the guanosine nucleoside from the RNA and DNA producing hydroxyguanosine, a marker associated with prostate cancer and tumor progression.[36] Alterations in tumor-related genes have been reported by a previous study. Prostate epithelial cells infected with ZIKV presented altered expression of innate immune response genes, such as the interferon at 6 dpi. At 21 dpi, a significant increase in the expression of genes involved in cell-cycle functions and prostate tumorigenesis was observed.[14] Additionally, miRNAs differentially expressed upon ZIKV infection in PNT1a cells showed in silico predictions correlated with inflammation, immunity, cell survival, and proliferation genes, with these potential targets enriched in Kegg cancer pathways.[15] Regarding the immune system, IFN-γ response, increased levels of other inflammatory cytokines (IL-1β, TNF-α), and ROS are related to prostatitis and ultimately linked to low-quality sperm and infertility.[37] Altogether, this suggests that the host cell response to prolonged ZIKV infection triggers inflammatory processes, which is corrobo-

https://doi.org/10.1021/acs.jproteome.2c00630
J. Proteome Res. 2023, 22, 193−203

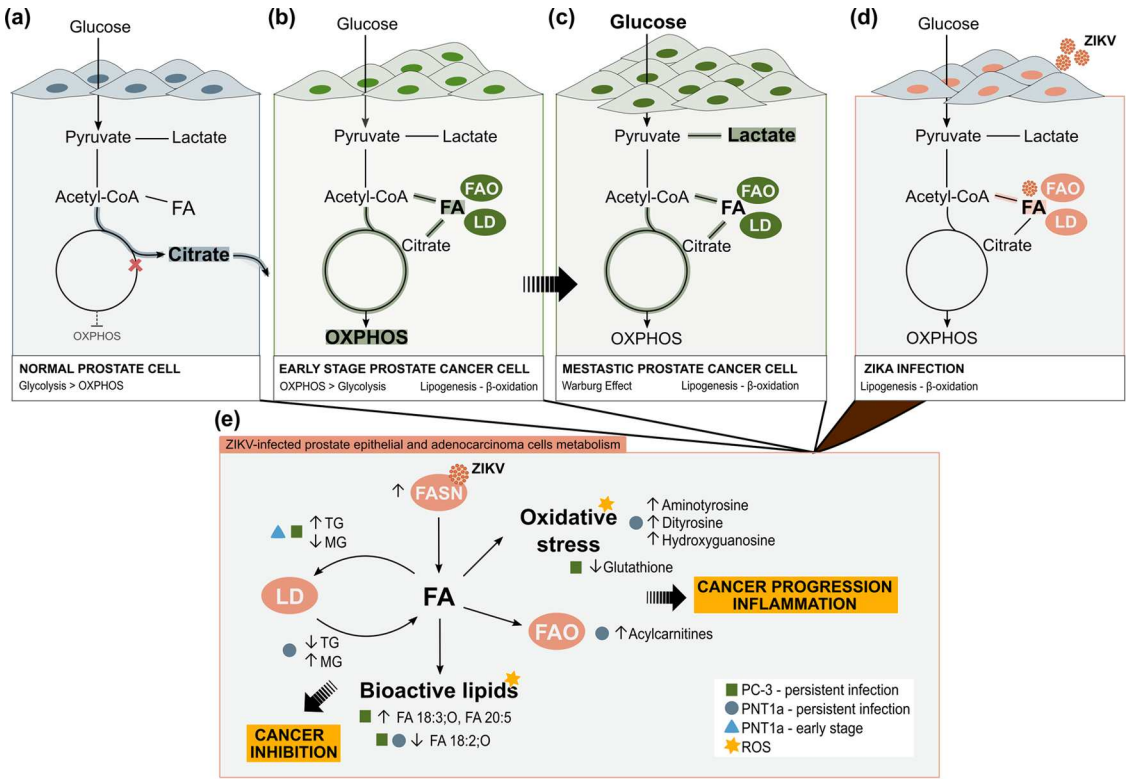

Figure 3. Cell metabolic states reported in the literature for normal epithelial prostate cells (A), early stage (B) and metastatic prostate cancer cells (C), and general ZIKV infection metabolic remodeling (D), highlighting the cell energetic state and lipid metabolism. Summary of the detected metabolite behavior and their importance in lipid metabolism in PNT1a and PC-3 under short and persistent Zika infection (E). Abbreviations: FA, fatty acid; FAO, fatty acid oxidation; LD, lipid droplet; MG, monoacylglycerol; OXPHOS, oxidative phosphorylation; ROS, reactive oxygen species; TG, triacylglycerol.

rated by prostatitis being a recurrent symptom associated with ZIKV infection in men.[13]

In contrast to PNT1a, we report prostate adenocarcinoma cells (PC-3) as more susceptible to cell death upon ZIKV-persistent infection, showing trends of cell proliferation inhibition already within 72 h. When comparing PC-3 metabolic alterations to PNT1a at 5 dpi, the increase in FA 18:3;0 and FA 20:5 is more pronounced in PC-3-infected cells. FA 20:5 (eicosapentaenoic acid) is a precursor of oxylipins, markers previously found altered in ZIKV-infected placentas.[31] It inhibits the phosphorylation of proline-rich tyrosine kinases (PYK2) and ERK and induces overproduction of ROS, exerting antiproliferative effects in PC-3. This anticancer effect has been pointed out by Oono et al. as dose-dependent, decreasing PC-3 cell proliferation, migration, and invasion.[38] Consistent with a potential increase of the ROS species, we observed a significant decrease in the antioxidant molecule glutathione ($\log_2$ FC = −3.02, p-value < 0.05) in PC-3 ZIKV-infected cells, while this marker was not even detected in PNT1a. The reduction of antioxidants may lead to apoptosis signaling.[39] Additionally, the oxylipin FA 18:3;0 could correspond to hydroxy-octadecatrienoic acid (HOTrE). Along with 13-HODE, 13-HOTrE stimulates PPAR-γ receptors, exhibiting anti-inflammatory properties, reducing the accumulation of lipid droplets, and inducing apoptosis.[40,41] Both HODE and HOTrE are metabolites of 15-LOX, an enzyme overexpressed in prostate normal cells but not in PC-3. However, PC-3 overexpresses PPAR-γ in contrast to normal cells.[41] Therefore, we hypothesize that oxylipins ligands of PPAR-γ may promote inhibition of cell proliferation in prostate cancer cells, but this effect may not be significant for normal cells.

ZIKV-Induced Lipid Metabolism Remodeling

Prostate cell metabolism is heavily influenced by intracellular zinc availability.[17] In the normal metabolic state (Figure 3A), high zinc concentrations inhibit mitochondrial aconitase, resulting in the accumulation of citrate and its cellular excretion to compose the seminal fluid. Considering that citrate is not available for oxidation in the TCA cycle and further generation of ATP by OXPHOS, prostate cells are considered energetically inefficient.[17−19] This metabolic state is shifted during the early stages of the malignancy process, where zinc availability is restricted and cancer cells can oxidize citrate for energy production (Figure 3B). Stocks of acetyl-CoA enable intensive lipid metabolism, promoting de novo lipogenesis and lipid accumulation as lipid droplets (LDs) in balance with increased fatty acid β-oxidation.[19−21] Later, prostate cancer cells will require extra energy input from anaerobic glycolysis to maintain the tumoral phenotype[17,18] (Figure 3C). Lipid metabolism is a key factor in cancer progression, contributing to energy production, alterations in membrane fluidity for increased invasiveness, and cell signaling, including apoptosis.[20,21,42] Lipid metabolism regulators, such as FASN, DGAT, and SREBP, have been found overexpressed in prostate cancer cells and, therefore, considered targets to constrain disease progression.[21,42]

Likewise, lipid metabolism is fundamentally altered by flavivirus infection and propagation. Flaviviruses induce cell lipogenesis to create fatty acids as substrates for β-oxidation and biosynthesis of more complex lipids; these will compose

https://doi.org/10.1021/acs.jproteome.2c00630
J. Proteome Res. 2023, 22, 193−203

membrane rearrangements, as well as accumulate in LDs[16,43] (Figure 3D). Conversely, drug therapies targeting key enzymes of lipid metabolism, such as FASN, DGAT, and SREBP, and the PPAR-γ receptor, have been pointed out as effective for both inhibition of flavivirus replication and cancer progression.[19,21,31,39,42−44] It has been reported that DENV and ZIKV manipulate SREBP pathways, regulating FASN, a key enzyme in fatty acid biosynthesis, and perturbing LD homeostasis.[45] The flavivirus nonstructural protein NS3 directly interacts with FASN, promoting its delocalization to sites of viral replication. By co-opting fatty acid biosynthesis to the endoplasmic reticulum (ER), flavivirus establishes an energetic source within replication complexes.[46] In ZIKV-infected placenta, FASN mRNA levels were found increased, suggesting the upregulation of this enzyme upon infection.[31] Fatty acid excess is cytotoxic for cells, and therefore, they are transformed into complex lipids such as TGs. TGs are formed by the action of DGAT and stored as lipid droplets derived from ER membranes.[31,43,45] While in infected placentas ZIKV induced DGAT upregulation and accumulation of LDs, other flavivirus and ZIKV are also known to promote lipophagy of LDs, consequently declining TG levels throughout the infection.[43,45,47] The initial increase in LDs has been associated with the stimulation of interferon response against Zika for infection control.[48]

We observed a significant increase in TGs in infected PNT1a cells at 5 dpi and a progressive decrease at 15 dpi. In contrast, MGs, subproducts of TG metabolism, and acylcarnitines presented an inverse trend (Figure 3E). These alterations are in accordance with the accumulation of TG in LDs in the first stages of infection followed by the expected lipophagy promoted by the flavivirus. Moreover, since LD accumulation is related to initial interferon activation, enhanced TG levels on the first few days of normal prostate cell infection could be linked to the observation of upregulation of interferon-related genes found by Izuagbe et al. at 6 dpi.[14] While normal prostate cells do not energetically depend on FASN, DGAT, and accumulation of LDs,[17−19] the competition for fatty acid biosynthesis and depletion of lipid storage may be significant and depreciative to prostate cancer cells. Acylcarnitines were found to decrease during the early days of infection in both PNT1a and PC-3. As the infection progresses, acylcarnitine's levels increase in PNT1a Zika-infected cells at 15 dpi, as a potential consequence of TG degradation to MG and FA observed with persistent infection. Acylcarnitines act as carriers of FAs to the mitochondria for β-oxidation. In prostate cancer, miRNAs modulate enzymes involved in the transport of carnitines, collaborating to control the intense FA load to the mitochondria.[49] It has been shown that Zika infection interferes with the mitochondria morphology, potentially causing its dysfunction.[6,31] Therefore, the increase of acylcarnitines over time may reflect Zika's interference with mitochondrial function.

CONCLUSIONS

Considering the cell metabolic remodeling promoted by ZIKV, as it superposes important characteristics of the basal metabolism of prostate normal and cancer cells, it is plausible to expect that these cells will behave metabolically differently upon infection. Additional studies to further investigate the effects of Zika infection in similar prostate and epithelial cell types are important to reinforce these findings and observe the nuances that differ in cell types as reservoirs for Zika replication. In general, the cell metabolic state of increased fatty acid synthesis, their storage as LDs, and metabolization by β-oxidation induced by ZIKV in normal cells are similar to the cellular state expected from prostate cancer; this conflict for resources may be a factor for cell proliferation inhibition. Conversely, ZIKV may be benefited through prostate epithelial cell metabolism, using citrate as a primary source for FA biogenesis. As the infection persists, we observed that PNT1a becomes more stressed, which perhaps contributes to cell malignancy, corroborating the trends of cancer upregulated pathways observed in previous studies of ZIKV persistence in prostate cells.[14,15] Overall, given the limitations of clinically available material to understand Zika's effect on the human prostate, in vitro studies shed light on potential mechanisms of cell metabolism remodeling upon infection and its dependence on the cell basal metabolic state.

ASSOCIATED CONTENT

Supporting Information

The Supporting Information is available free of charge at https://pubs.acs.org/doi/10.1021/acs.jproteome.2c00630.

Elucidation data of additional biomarkers through mass spectrometry; PLS-DA score plots at 5, 10, and 15 dpi for PNT1a Zika-infected and mock cells (Figure S1); volcano plots at 5, 10, and 15 dpi time points for PNT1a cells (Figure S2); PLS-DA score plot at 5 dpi for PC-3 Zika-infected cells and mock cells (Figure S3); volcano plot at 5 dpi for PC-3 cells (Figure S4); annotated metabolites for PNT1a cells at 5, 10, and 15 dpi (Table S1); annotated metabolites for PNT1a and PC-3 cells at 5 dpi (Table S2); and mass spectrometry data available at Zenodo on this link: 10.5281/zenodo.7334362 (PDF)

AUTHOR INFORMATION

Corresponding Author

Rodrigo R. Catharino − *Innovare Biomarkers Laboratory, School of Pharmaceutical Sciences, University of Campinas, Campinas, SP 13083-970, Brazil;* orcid.org/0000-0001-7219-2644; Phone: +55 19 3521-9138; Email: rrc@unicamp.br

Authors

Jeany Delafiori − *Innovare Biomarkers Laboratory, School of Pharmaceutical Sciences, University of Campinas, Campinas, SP 13083-970, Brazil*

Alessandra V. de S. Faria − *Department of Biochemistry and Tissue Biology, University of Campinas, Campinas, SP 13083-862, Brazil*

Arthur N. de Oliveira − *Innovare Biomarkers Laboratory, School of Pharmaceutical Sciences, University of Campinas, Campinas, SP 13083-970, Brazil*

Geovana M. Sales − *Innovare Biomarkers Laboratory, School of Pharmaceutical Sciences, University of Campinas, Campinas, SP 13083-970, Brazil*

Flávia Luísa Dias-Audibert − *Innovare Biomarkers Laboratory, School of Pharmaceutical Sciences, University of Campinas, Campinas, SP 13083-970, Brazil*

Complete contact information is available at: https://pubs.acs.org/10.1021/acs.jproteome.2c00630

https://doi.org/10.1021/acs.jproteome.2c00630
J. Proteome Res. 2023, 22, 193−203

Author Contributions

Conceptualization: J.D., A.V.S.F., and R.R.C. Methodology: J.D. and A.V.S.F. Formal analysis: J.D., A.V.S.F., F.L.D.-A., A.N.O., and G.M.S. Investigation: J.D. Data Curation: J.D. and R.R.C. Writing—original draft preparation: J.D. Writing—review & editing: A.V.S.F., G.M.S., A.N.O., and R.R.C. Supervision: R.R.C. All authors read and approved the final manuscript.

Notes

The authors declare no competing financial interest.

■ ACKNOWLEDGMENTS

The authors would like to thank the network involved in providing cell lineages and Zika strain and Thermo Scientific and LADETEC (UFRJ) for the technical support. The authors are grateful to Dr. Carmen Veríssima Ferreira-Halder and Dr. José Luiz Proença-Módena for their generosity in making their lab infrastructure available for virus and cellular assays. This work was supported by the São Paulo Research Foundation (FAPESP) [2019/05718-3 to J.D. and 2017/08119-8 to A.V.S.F.], the Coordination for the Improvement of Higher Education Personnel (CAPES) [88887.513974/2020-00 to A.N.O. and 88882.329849/2010-01 to G.M.S.], and the National Council for Scientific and Technological Development (CNPq) [141200/2018-9 to FLD-A].

■ ABBREVIATIONS USED

CAR, acylcarnitine; DG, diacylglycerol; dpi, days post infection; FA, fatty acid; FAO, fatty acid oxidation; FC, fold change; CCR2, HODE, hydroxy-decadienoic acid; HOTrE, hydroxy-octadecatrienoic acid; LD, lipid droplet; MG, monoacylglycerol; MOI, multiplicity of infection; MTT, 3-(4,5-dimethylthiazol-2-yl)-2,5-diphenyltetrazolium bromide; OXPHOS, oxidative phosphorylation; PCA, principal component analysis; PLS-DA, partial least-square discriminant analysis; ROS, reactive oxygen species; TCA cycle, tricarboxylic acid cycle; TG, triacylglycerol; ZIKV, Zika virus

■ REFERENCES

(1) Dick, G. W. A. Zika Virus (II). Pathogenicity and Physical Properties. *Trans. R. Soc. Trop. Med. Hyg.* **1952**, *46*, 521−534.

(2) Petersen, L. R.; Jamieson, D. J.; Powers, A. M.; Honein, M. A. Zika Virus (Review Article). *N. Engl. J. Med.* **2016**, *374*, 1552−1563.

(3) Boeuf, P.; Drummer, H. E.; Richards, J. S.; Scoullar, M. J. L.; Beeson, J. G. The Global Threat of Zika Virus to Pregnancy: Epidemiology, Clinical Perspectives, Mechanisms, and Impact. *BMC Med.* **2016**, *14*, 112.

(4) Zhu, Z.; Gorman, M. J.; McKenzie, L. D.; Chai, J. N.; Hubert, C. G.; Prager, B. C.; Fernandez, E.; Richner, J. M.; Zhang, R.; Shan, C.; Tycksen, E.; Wang, X.; Shi, P. Y.; Diamond, M. S.; Rich, J. N.; Chheda, M. G. Zika Virus Has Oncolytic Activity against Glioblastoma Stem Cells. *J. Exp. Med.* **2017**, *214*, 2843−2857.

(5) Chen, Q.; Wu, J.; Ye, Q.; Ma, F.; Zhu, Q.; Wu, Y.; Shan, C.; Xie, X.; Li, D.; Zhan, X.; Li, C.; Li, X. F.; Qin, X.; Zhao, T.; Wu, H.; Shi, P. Y.; Man, J.; Qin, C. F. Treatment of Human Glioblastoma with a Live Attenuated Zika Virus Vaccine Candidate. *mBio* **2018**, *9*, e01683−e01718.

(6) Garcez, P. P.; Loiola, E. C.; da Costa, R. M.; Higa, L. M.; Trindade, P.; Delvecchio, R.; Nascimento, J. M.; Brindeiro, R.; Tanuri, A.; Rehen, S. K. Zika Virus: Zika Virus Impairs Growth in Human Neurospheres and Brain Organoids. *Science* **2016**, *352*, 816−818.

(7) Kaid, C.; Goulart, E.; Caires-Júnior, L. C.; Araujo, B. H. S.; Soares-Schanoski, A.; Bueno, H. M. S.; Telles-Silva, K. A.; Astray, R. M.; Assoni, A. F.; Júnior, A. F. R.; Ventini, D. C.; Puglia, A. L. P.; Gomes, R. P.; Zatz, M.; Okamoto, O. K. Zika Virus Selectively Kills Aggressive Human Embryonal CNS Tumor Cells in Vitro and in Vivo. *Cancer Res.* **2018**, *78*, 3363−3374.

(8) Iannolo, G.; Sciuto, M. R.; Cuscino, N.; Pallini, R.; Douradinha, B.; Ricci Vitiani, L.; de Maria, R.; Conaldi, P. G. Zika Virus Infection Induces MiR34c Expression in Glioblastoma Stem Cells: New Perspectives for Brain Tumor Treatments. *Cell Death Dis.* **2019**, *10*, 263.

(9) Liang, Q.; Luo, Z.; Zeng, J.; Chen, W.; Foo, S. S.; Lee, S. A.; Ge, J.; Wang, S.; Goldman, S. A.; Zlokovic, Bv.; Zhao, Z.; Jung, J. U. Zika Virus NS4A and NS4B Proteins Deregulate Akt-MTOR Signaling in Human Fetal Neural Stem Cells to Inhibit Neurogenesis and Induce Autophagy. *Cell Stem Cell* **2016**, *19*, 663−671.

(10) Dabaja, M. Z.; Lima, E. de O.; de Oliveira, D. N.; Guerreiro, T. M.; Melo, C. F. O. R.; Morishita, K. N.; Lancellotti, M.; Ruiz, A. L. T. G.; Goulart, G.; Duarte, D. A.; Catharino, R. R. Metabolic Alterations Induced by Attenuated Zika Virus in Glioblastoma Cells. *Cell Biosci.* **2018**, *8*, 47.

(11) Paz-Bailey, G.; Rosenberg, E. S.; Doyle, K.; Munoz-Jordan, J.; Santiago, G. A.; Klein, L.; Perez-Padilla, J.; Medina, F. A.; Waterman, S. H.; Adams, L. E.; Lozier, M. J.; Bertrán-Pasarell, J.; Garcia Gubern, C.; Alvarado, L. I.; Sharp, T. M. Persistence of Zika Virus in Body Fluids — Final Report. *N. Engl. J. Med.* **2018**, *379*, 1234−1243.

(12) Spencer, J. L.; Lahon, A.; Tran, L. L.; Arya, R. P.; Kneubehl, A. R.; Vogt, M. B.; Xavier, D.; Rowley, D. R.; Kimata, J. T.; Rico-Hesse, R. R. Replication of Zika Virus in Human Prostate Cells: A Potential Source of Sexually Transmitted Virus. *J. Infect. Dis.* **2018**, *217*, 538−547.

(13) Oliveira, D. B. L.; Durigon, G. S.; Mendes, É. A.; Ladner, J. T.; Andreata-Santos, R.; Araujo, D. B.; Botosso, V. F.; Paola, N. D.; Neto, D. F. L.; Cunha, M. P.; Braconi, C. T.; Alves, R. P. S.; Jesus, M. R.; Pereira, L. R.; Melo, S. R.; Mesquita, F. S.; Silveira, V. B.; Thomazelli, L. M.; Favoretto, S. R.; Almonfrey, F. B.; Abdulkader, R. C. R. M.; Gabrili, J. M.; Tambourgi, Dv.; Oliveira, S. F.; Prieto, K.; Wiley, M. R.; Ferreira, L. C. S.; Silva, Mv.; Palacios, G. F.; Zanotto, P. M. A.; Durigon, E. L. Persistence and Intra-Host Genetic Evolution of Zika Virus Infection in Symptomatic Adults: A Special View in the Male Reproductive System. *Viruses* **2018**, *10*, 615.

(14) Izuagbe, R. E. A Prostate Cell Line Model of Persistent Zika Virus Infection. Master Dissertation, Queensland University of Technology: Brisbane, Australia, 2019. https://eprints.qut.edu.au/129570/ (Accessed 11/10/2022).

(15) Machado, F. C.; Bittar, C.; Rahal, P.; Calmon, M. F. Identification of Differentially Expressed MiRNAs in Human Cells Infected with Different Zika Virus Strains. *Arch. Virol.* **2021**, *166*, 1681−1689.

(16) Byers, N. M.; Fleshman, A. C.; Perera, R.; Molins, C. R. Metabolomic Insights into Human Arboviral Infections: Dengue, Chikungunya, and Zika Viruses. *Viruses* **2019**, *11*, 225.

(17) Eidelman, E.; Twum-Ampofo, J.; Ansari, J.; Siddiqui, M. M. The Metabolic Phenotype of Prostate Cancer. *Front. Oncol.* **2017**, *7*, 131.

(18) Cutruzzolà, F.; Giardina, G.; Marani, M.; Macone, A.; Paiardini, A.; Rinaldo, S.; Paone, A. Glucose Metabolism in the Progression of Prostate Cancer. *Front. Physiol.* **2017**, *8*, 97.

(19) Elia, I.; Schmieder, R.; Christen, S.; Fendt, S. M. Organ-Specific Cancer Metabolism and Its Potential for Therapy. In *Handbook of Experimental Pharmacology*, Springer: Cham, 2016; Vol. *233*, pp 321−353.

(20) Liu, Y. Fatty Acid Oxidation Is a Dominant Bioenergetic Pathway in Prostate Cancer. *Prostate Cancer Prostatic Dis.* **2006**, *9*, 230−234.

(21) Xu, H.; Chen, Y.; Gu, M.; Liu, C.; Chen, Q.; Zhan, M.; Wang, Z. Fatty Acid Metabolism Reprogramming in Advanced Prostate Cancer. *Metabolites* **2021**, *11*, 765.

(22) Meertens, L.; Labeau, A.; Dejarnac, O.; Cipriani, S.; Sinigaglia, L.; Bonnet-Madin, L.; le Charpentier, T.; Hafirassou, M. L.; Zamborlini, A.; Cao-Lormeau, V. M.; Coulpier, M.; Missé, D.;

https://doi.org/10.1021/acs.jproteome.2c00630
J. Proteome Res. 2023, 22, 193−203

Jouvenet, N.; Tabibiazar, R.; Gressens, P.; Schwartz, O.; Amara, A. Axl Mediates ZIKA Virus Entry in Human Glial Cells and Modulates Innate Immune Responses. *Cell Rep.* **2017**, *18*, 324−333.
(23) Silva-Filho, J. L.; de Oliveira, L. G.; Monteiro, L.; Parise, P. L.; Zanluqui, N. G.; Polonio, C. M.; de Freitas, C. L.; Toledo-Teixeira, D. A.; de Souza, W. M.; Bittencourt, N.; Amorim, M. R.; Forato, J.; Muraro, S. P.; de Souza, G. F.; Martini, M. C.; Bispo-dos-Santos, K.; Vieira, A.; Judice, C. C.; Pastore, G. M.; Amaral, E.; Passini Junior, R.; Mayer-Milanez, H. M. B. P.; Ribeiro-do-Valle, C. C.; Calil, R.; Renato Bennini Junior, J.; Lajos, G. J.; Altemani, A.; Nolasco da Silva, M. T.; Carolina Coan, A.; Francisca Colella-Santos, M.; von Zuben, A. P. B.; Vinolo, M. A. R.; Arns, C. W.; Catharino, R. R.; Costa, M. L.; Angerami, R. N.; Freitas, A. R. R.; Resende, M. R.; Garcia, M. T.; Luiza Moretti, M.; Renia, L.; Ng, L. F. P.; Rothlin, Cv.; Costa, F. T. M.; Peron, J. P. S.; Proença-Modena, J. L. Gas6 Drives Zika Virus-Induced Neurological Complications in Humans and Congenital Syndrome in Immunocompetent Mice. *Brain Behav. Immun.* **2021**, *97*, 260−274.
(24) Sharp, T. M.; Fischer, M.; Muñoz-Jordán, J. L.; Paz-Bailey, G.; Erin Staples, J.; Gregory, C. J.; Waterman, S. H. Dengue and Zika Virus Diagnostic Testing for Patients with a Clinically Compatible Illness and Risk for Infection with Both Viruses. *MMWR Recomm. Rep.* **2019**, *68*, 1.
(25) Kuivanen, S.; Bespalov, M. M.; Nandania, J.; Ianevski, A.; Velagapudi, V.; de Brabander, J. K.; Kainov, D. E.; Vapalahti, O. Obatoclax, Saliphenylhalamide and Gemcitabine Inhibit Zika Virus Infection in Vitro and Differentially Affect Cellular Signaling, Transcription -and Metabolism. *Antiviral Res.* **2017**, *139*, 117−128.
(26) Melo, C. F. O. R.; Navarro, L. C.; de Oliveira, D. N.; Guerreiro, T. M.; Lima, E. de O.; Delafiori, J.; Dabaja, M. Z.; Ribeiro, M. da S.; de Menezes, M.; Rodrigues, R. G. M.; Morishita, K. N.; Esteves, C. Z.; de Amorim, A. L. L.; Aoyagui, C. T.; Parise, P. L.; Milanez, G. P.; do Nascimento, G. M.; Ribas Freitas, A. R.; Angerami, R.; Costa, F. T. M.; Arns, C. W.; Resende, M. R.; Amaral, E.; Junior, R. P.; Ribeiro-do-Valle, C. C.; Milanez, H.; Moretti, M. L.; Proenca-Modena, J. L.; Avila, S.; Rocha, A.; Catharino, R. R.; Altemani, A.; Coan, A. C.; Barnabé, A. C. de S.; da Soledade, A. L. R.; de Moraes, A. P.; von Zuben, A. P. B.; Judice, C. C.; Teixeira, D. A. de T.; de Morais, É. R.; Santos, F. R.; Lajos, G. J.; Pastore, G. M.; Bennini Júnior, J. R.; Leite, J. A.; Fertrin, K. Y.; Caserta, L. C.; Garcia, M. T.; Vinolo, M. A. R.; da Silva, M. T. N.; Colella-Santos, M. F.; Costa, M. L.; Calil, R.; de Paula, R. F. de O. A Machine Learning Application Based in Random Forest for Integrating Mass Spectrometry-Based Metabolomic Data: A Simple Screening Method for Patients with Zika Virus. *Front. Bioeng. Biotechnol.* **2018**, *6*, 31.
(27) Delafiori, J.; Lima, E. de O.; Dabaja, M. Z.; Dias-Audibert, F. L.; de Oliveira, D. N.; Melo, C. F. O. R.; Morishita, K. N.; Sales, G. M.; Ruiz, A. L. T. G.; da Silva, G. G.; Lancellotti, M.; Catharino, R. R. Molecular Signatures Associated with Prostate Cancer Cell Line (PC-3) Exposure to Inactivated Zika Virus. *Sci Rep.* **2019**, *9*, No. 15351.
(28) Nunes, E. da C.; de Filippis, A. M. B.; Pereira, T. D. E. S.; Faria, N. R. da C.; Salgado, Á.; Santos, C. S.; Carvalho, T. C. P. X.; Calcagno, J. I.; Chalhoub, F. L. L.; Brown, D.; Giovanetti, M.; Alcantara, L. C. J.; Barreto, F. K.; de Siqueira, I. C.; Canuto, G. A. B. Untargeted Metabolomics Insights into Newborns with Congenital Zika Infection. *Pathogens.* **2021**, *10*, 468.
(29) Pang, Z.; Chong, J.; Li, S.; Xia, J. Metaboanalystr 3.0: Toward an Optimized Workflow for Global Metabolomics. *Metabolites* **2020**, *10*, 186.
(30) Stassen, L.; Armitage, C. W.; Van der Heide, D. J.; Beagley, K. W.; Frentiu, F. D. Zika Virus in the Male Reproductive Tract. *Viruses.* **2018**, *10*, 198.
(31) Chen, Q.; Gouilly, J.; Ferrat, Y. J.; Espino, A.; Glaziou, Q.; Cartron, G.; el Costa, H.; Al-Daccak, R.; Jabrane-Ferrat, N. Metabolic Reprogramming by Zika Virus Provokes Inflammation in Human Placenta. *Nat Commun.* **2020**, *11*, No. 2967.
(32) Faria, N. R. d. C.; Chaves-Filho, A. B.; Alcantara, L. C. J.; de Siqueira, I. C.; Calcagno, J. I.; Miyamoto, S.; de Filippis, A. M. B.; Yoshinaga, M. Y. Plasma Lipidome Profiling of Newborns with Antenatal Exposure to Zika Virus. *PLoS Negl. Trop. Dis.* **2021**, *15*, No. e0009388.
(33) Catala, A.; Stone, M.; Busch, M. P.; D'Alessandro, A. Reprogramming of Red Blood Cell Metabolism in Zika Virus−Infected Donors. *Transfusion* **2022**, *62*, 1045.
(34) Zhan, X.; Wang, X.; Desiderio, D. M. Mass Spectrometry Analysis of Nitrotyrosine-Containing Proteins. *Mass Spectrom Rev.* **2015**, *34*, 423−448.
(35) Campolo, N.; Issoglio, F. M.; Estrin, D. A.; Bartesaghi, S.; Radi, R. 3-Nitrotyrosine and Related Derivatives in Proteins: Precursors, Radical Intermediates and Impact in Function. *Essays Biochem.* **2020**, *64*, 111−133.
(36) Ohtake, S.; Kawahara, T.; Ishiguro, Y.; Takeshima, T.; Kuroda, S.; Izumi, K.; Miyamoto, H.; Uemura, H. Oxidative Stress Marker 8-Hydroxyguanosine Is More Highly Expressed in Prostate Cancer than in Benign Prostatic Hyperplasia. *Mol. Clin. Oncol.* **2018**, *9*, 302−304.
(37) Motrich, R. D.; Salazar, F. C.; Breser, M. L.; Mackern-Oberti, J. P.; Godoy, G. J.; Olivera, C.; Paira, D. A.; Rivero, V. E. Implications of Prostate Inflammation on Male Fertility. *Andrologia* **2018**, *50*, No. e13093.
(38) Oono, K.; Ohtake, K.; Watanabe, C.; Shiba, S.; Sekiya, T.; Kasono, K. Contribution of Pyk2 Pathway and Reactive Oxygen Species (ROS) to the Anti-Cancer Effects of Eicosapentaenoic Acid (EPA) in PC3 Prostate Cancer Cells. *Lipids Health Dis.* **2020**, *19*, 15.
(39) Tang, D. G.; La, E.; Kern, J.; Kehrer, J. P. Fatty Acid Oxidation and Signaling in Apoptosis. *Biol. Chem.* **2002**, *383*, 425−442.
(40) Pauls, S. D.; Rodway, L. A.; Winter, T.; Taylor, C. G.; Zahradka, P.; Aukema, H. M. Anti-Inflammatory Effects of α-Linolenic Acid in M1-like Macrophages Are Associated with Enhanced Production of Oxylipins from α-Linolenic and Linoleic Acid. *J. Nutr. Biochem.* **2018**, *57*, 121−129.
(41) Subbarayan, V.; Xu, X. C.; Kim, J.; Yang, P.; Hoque, A.; Sabichi, A. L.; Llansa, N.; Mendoza, G.; Logothetis, C. J.; Newman, R. A.; Lippman, S. M.; Menter, D. G. Inverse Relationship between 15-Lipoxygenase-2 and PPAR-γ Gene Expression in Normal Epithelia Compared with Tumor Epithelia. *Neoplasia* **2005**, *7*, 280−293.
(42) Mitra, R.; Le, T. T.; Gorjala, P.; Goodman, O. B. Positive Regulation of Prostate Cancer Cell Growth by Lipid Droplet Forming and Processing Enzymes DGAT1 and ABHD5. *BMC Cancer* **2017**, *17*, 631.
(43) Martín-Acebes, M. A.; Vázquez-Calvo, Á.; Saiz, J. C. Lipids and Flaviviruses, Present and Future Perspectives for the Control of Dengue, Zika, and West Nile Viruses. *Prog. Lipid Res.* **2016**, *64*, 123−137.
(44) Mwaliko, C.; Nyaruaba, R.; Zhao, L.; Atoni, E.; Karungu, S.; Mwau, M.; Lavillette, D.; Xia, H.; Yuan, Z. Zika Virus Pathogenesis and Current Therapeutic Advances. *Pathog. Glob. Health.* **2021**, *115*, 21−39.
(45) Cloherty, A. P. M.; Olmstead, A. D.; Ribeiro, C. M. S.; Jean, F. Hijacking of Lipid Droplets by Hepatitis C, Dengue and Zika Viruses-from Viral Protein Moonlighting to Extracellular Release. *Int. J. Mol. Sci.* **2020**, *21*, 7901.
(46) Heaton, N. S.; Perera, R.; Berger, K. L.; Khadka, S.; LaCount, D. J.; Kuhn, R. J.; Randall, G. Dengue Virus Nonstructural Protein 3 Redistributes Fatty Acid Synthase to Sites of Viral Replication and Increases Cellular Fatty Acid Synthesis. *Proc. Natl. Acad. Sci. U.S.A.* **2010**, *107*, 17345−17350.
(47) Leier, H. C.; Weinstein, J. B.; Kyle, J. E.; Lee, J. Y.; Bramer, L. M.; Stratton, K. G.; Kempthorne, D.; Navratil, A. R.; Tafesse, E. G.; Hornemann, T.; Messer, W. B.; Dennis, E. A.; Metz, T. O.; Barklis, E.; Tafesse, F. G. A Global Lipid Map Defines a Network Essential for Zika Virus Replication. *Nat Commun.* **2020**, *11*, No. 3652.
(48) Monson, E. A.; Crosse, K. M.; Duan, M.; Chen, W.; O'Shea, R. D.; Wakim, L. M.; Carr, J. M.; Whelan, D. R.; Helbig, K. J. Intracellular Lipid Droplet Accumulation Occurs Early Following Viral Infection and Is Required for an Efficient Interferon Response. *Nat Commun.* **2021**, *12*, No. 4303.
(49) Valentino, A.; Calarco, A.; di Salle, A.; Finicelli, M.; Crispi, S.; Calogero, R. A.; Riccardo, F.; Sciarra, A.; Gentilucci, A.; Galderisi, U.;

https://doi.org/10.1021/acs.jproteome.2c00630
J. Proteome Res. 2023, 22, 193−203

Margarucci, S.; Peluso, G. Deregulation of MicroRNAs Mediated Control of Carnitine Cycle in Prostate Cancer: Molecular Basis and Pathophysiological Consequences. *Oncogene* **2017**, *36*, 6030−6040.

https://doi.org/10.1021/acs.jproteome.2c00630
J. Proteome Res. 2023, 22, 193−203